The 9th European Congress on Computational Methods in Applied Sciences and Engineering
ECCOMAS Congress 2024
3–7 June 2024, Lisboa, Portugal

LOCAL IMMERSED BOUNDARY METHOD ON BODY-CONFORMAL GRIDS FOR THE CAPTURE OF GEOMETRICAL FEATURES IN AERODYNAMIC SIMULATIONS

Rayan Nkenfack Soppi[1,2], Francesca Basile[2], Stéphanie Péron[2], Massyl Lagha[1] and Imadeddine Hammani[2]

[1] AIRBUS, 314 Route de Bayonne, Toulouse 31000, France
e-mails: rayan.nkenfack@airbus.com, massyl.lagha@airbus.com

[2] ONERA - Université Paris Saclay, Châtillon 92322, France
emails: rayan.nkenfack_soppi@onera.fr, francesca.basile@onera.fr, stephanie.peron@onera.fr, imadeddine.hammani@onera.fr

Key words: Immersed Boundary Method, Mesh adaptation, Icing

Summary. This paper presents a Local Immersed Boundary Method (LIBM) applied on curvilinear grids to simulate turbulent flows around obstacles with geometrical complex details. With this approach, the governing equations are solved with a finite volume solver using a wall-resolved technique over the body-conformal region of the mesh, whereas an Immersed Boundary Method (IBM) is applied to account for the complex geometrical details. The IBM method consists in forcing the solution through a wall function at some discretizations points close to the immersed details. When the background mesh is too coarse in the vicinity of the immersed obstacles, mesh adaptation is performed to properly capture the flow physics induced by the presence of the immersed obstacle. The preprocessing is achieved with Cassiopée modules and the flow simulation is performed by solving the compressible Reynolds-Averaged Navier-Stokes (RANS) equations with the flow solver CODA (CFD for ONERA-DLR-AIRBUS) [1]. This approach has been applied to simulate turbulent flows around a 2D multi-element airfoil. The results obtained show that the local IBM approach is an efficient method to deal with geometrical complex obstacles as it allows a significant reduction of the mesh generation effort without compromising the flow solution accuracy.

1 INTRODUCTION

The growth in computational power resources coupled with the increase in robustness and accuracy of numerical solvers witnessed over the last few decades have made Computational Fluid Dynamics (CFD) an increasingly important part of aircraft design. As a result, Reynolds-Averaged Navier-Stokes (RANS) simulations on body-conformal meshes are commonly performed to asses the aerodynamic properties of aerospace vehicles. However, for realistic aircraft configurations with complex geometries, the mesh generation step is time-consuming. It requires manual interaction, expertise and therefore represents the bottleneck of the CFD workflow. This

[1]CODA is a CFD software jointly developed by ONERA, DLR, Airbus and their European research partners. CODA belongs to ONERA, DLR and Airbus.

issue becomes even more important in the pre-design phases due to the large number of potential configurations. Low-fidelity CFD tools (lifting-line, panel method, etc.) are usually used at these stages to quickly get aerodynamic performance trends, but these models are limited by numerous flow assumptions. The aim of the present work is to propose a mid-fidelity CFD tool based on RANS simulations with a local immersed boundary approach, in order to alleviate the mesh generation effort around geometrical complex obstacles. Unlike the body-fitted approach, IBM simulations are performed on meshes that do not conform to the obstacle shape. As a results, IB methods seems to be well suited to overcome the aforementioned grids constraints for complex geometries.

The IBM concept was first introduced by Peskin [15] to simulate blood flow in the cardiovascular system. Since then, many variants of this method have been developed to simulate a wide range of flow problem. Mittal and Iaccarino [8] classified these variants in two families: the continuous forcing approach and the discrete forcing approach. The former consists of introducing a source term in the governing equations in order to mimic the effect of the immersed obstacle on the flow. This approach is well suited for immersed elastic boundaries with low Reynolds number, but can lead to severe stability constraints as well as lack of accuracy in a presence of rigid bodies [8]. Moreover, the smoothing functions used in this approach to ensure a gradual switch between fluid and solid regions also leads to an inability to provide a sharp representation of the IB, which is undesirable for high Reynolds number flows [8]. The latter consists of a direct imposition of the flow solution at some discretizations points close to the immersed walls, is suitable for rigid bodies and high Reynolds number flows as no smoothing function is required at the fluid-solid interface. However, this approach is less suitable for moving IB, as IBM preprocessing should be performed at each flow solver iteration to update the location of the forcing points with respect to the IB motion.

Another way of categorizing IB methods is according to whether they are intended to be used at a local or a global level. With the global approach the IB method is applied to the entire obstacle, whereas in the local approach only geometrical details are taken into account by the IB method. In the literature, IBM is usually applied to the whole obstacle within a Cartesian mesh [18, 14, 4, 12]. The main advantages of Cartesian grids are ease of mesh generation and computational efficiency (memory and CPU savings), especially when simulations are carried out using Cartesian solvers. However, for unstructured industrial solvers, Cartesian mesh topology is not suitable due the large number of cells required to simulate high Reynolds number flows. In fact, for wall-bounded turbulent flows, it is desirable to use a mesh topology with grid lines aligned with streamlines. This makes it possible to use high aspect ratio cells at the walls instead of being constrained by isotropic cells with a Cartesian mesh, and therefore leads to a significant reduction in the overall cell count of the body-conformal grid compared to a Cartesian grid. Various studies [10, 6, 16] have demonstrated that it could be advantageous to apply IBM on body-conformal grids. Wei Jun Zhu *et al.* [21] have applied Local Immersed Boundary Method (LIBM) on a curvilinear grid to simulate the turbulent flow past an airfoil with moving trailing-edge flap using URANS simulations. Similar work was carried out by Loïc Mochel *et al.* [9] to take in account technological effect on a simplified space launcher after-body using Zonal Detached Eddy Simulations (ZDES).

The goal of the present work is to demonstrate the ability of a local IBM approach to properly take into account geometrical details such as slat and flap in a body-conformal mesh using RANS simulations. The relevance of an LIBM technique lies in its ability to take advantage of both IB and body-fitted methods: reduction of the mesh generation effort around geometrical complex details and good solution accuracy, since the boundary layer is resolved in the body-conformal region of the mesh.

2 DESCRIPTION OF THE WORKFLOW

The workflow of the LIBM technique presented in this paper is divided in two main stages: the preprocessing and the flow simulation.

2.1 Preprocessing

The whole preprocessing is achieved with modules from the pre-/post-processing library Cassiopée [2] and is divided in three steps: the mesh adaptation, the blanking and the location of IBM points.

2.1.1 Mesh adaptation

In the present LIBM approach, the geometrical detail is immersed in a pre-existing hexahedral body-conformal grid. Unlike Cartesian grids, the cells anisotropy of body-conformal grids allows a significant cell count saving when simulating high-Reynolds number flows. However, as the mesh resolution decreases rapidly with respect to the wall distance, the cell size of the initial mesh is usually too coarse to properly capture the geometry and the flow physics induced by the immersed obstacle. When this happens, a hierarchical mesh adaptation is performed in the vicinity of the immersed obstacle. At each iteration of the adaptation process, a region of cells to be adapted is defined considering the first three layers of fluid cells and the first two layers of solid cells as shown in Fig 1a. Since in our LIBM approach, the IBM forcing points are located at a certain distance H from the IB (see section 2.2.2 for details), the region of cells to be adapted is defined with respect to an offset of the real IB. The misalignment between the grid lines of the initial mesh and the IB, as well as the anisotropic nature of the cells in the initial mesh implies the use of a characteristic cell size h_c as a metric to assess the mesh resolution at each iteration. The process of isotropic mesh adaptation continues until the mesh resolution close to the front of IBM forcing points (fluid-solid interface) becomes fine enough to satisfy the grid requirements for the application of a wall model. The main parameters of the mesh adaptation are the number of layers of fluid cells used to define the region of cells to be adapted and the metric h_c. The expression of h_c given in (1) is defined for 2D cases only.

$$h_c = \sqrt{\max(S_i)}, \quad i = 1, 2, 3, .., N \tag{1}$$

Where N is the number of cells to be adapted and S_i the area of cell i in the region of cells to adapted.

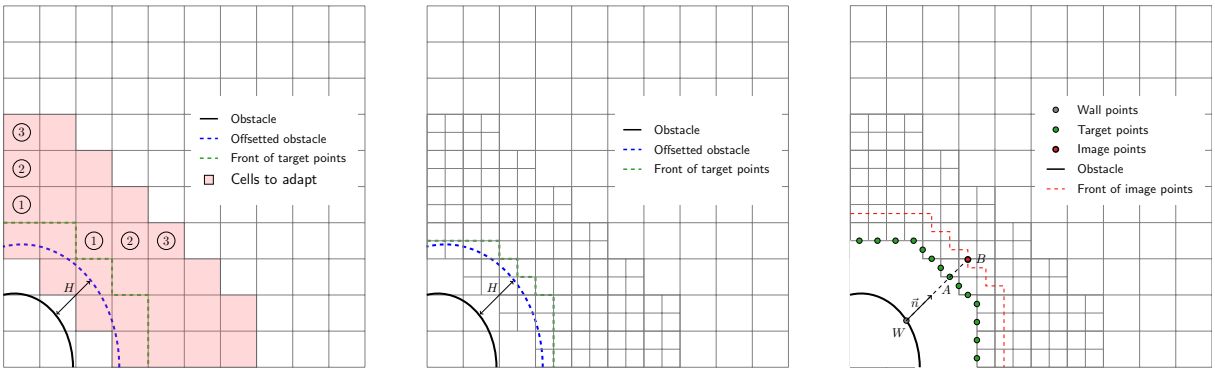

(a) Initial mesh (b) Adapted mesh (c) Blanked mesh

Figure 1: Preprocessing steps

2.1.2 Blanking and location of IBM points

The Immersed Boundary Method applied in this paper is derived from the ghost-cell direct forcing formulation proposed in [18] and [5]. The computational domain is split into solid and fluid regions using a blanking algorithm. A cell is marked solid if at least one of its nodes lies inside the immersed obstacle. Solid cells are removed from the mesh after the blanking, resulting in a staircase path in the vicinity of the obstacle. The immersed boundary condition is imposed at IB target points located at the face centers of the staircase border. Each target point is associated with an image point in the fluid region and a wall point in the solid region. Image and wall points are constructed by projecting the target points along the normal to the wall, either in the fluid domain (for image points) or in the solid domain (for wall points).

Several studies on IBM with the direct forcing formulation have pointed out the major role of IB points location on the method accuracy [17, 3, 4]. In the present paper, IB target points location corresponds the one proposed by Constant *et al.* [4] which ensures to have target points in the logarithmic sub-layer of the turbulent boundary layer. This prevents the wall model from being applied in the buffer region which is not well represented by most analytical wall model, and also in the viscous sub-layer in order to avoid possible inconsistencies between the mesh resolution and the wall model (due to the strong tangential velocity gradients in the near-wall region) which leads to spurious oscillations on skin pressure and friction coefficient as observed in [17, 3, 4]. In practice, this means moving the front of target points away from the wall by a distance H called the modelling height. Then, all fluid cells with a wall distance to the immersed obstacle less than H are also blanked and removed from the mesh. The modelling height H is computed using turbulent boundary layer assumptions on a flat plate and depends on the Reynolds number and the desired y^+_{target} value at target points. y^+_{target} is a user-defined quantity and is usually chosen in the range 100 - 300, which corresponds to the logarithmic region of the boundary layer.

$$H = \sqrt{2}\frac{y^+_{\text{target}}\, L}{Re\sqrt{f(Re)}}, \tag{2}$$

with :

$$f(Re) = 0.058Re^{-0.2} \tag{3}$$

L is the characteristic length of the initial obstacle (without the immersed detail).

2.2 Flow simulation

2.2.1 Governing equations

The steady-state mean flow is obtained by solving the compressible RANS equations within the Finite Volume (FV) framework, using the industrial solver CODA [20].

$$\begin{cases} \frac{\partial \rho}{\partial t} + \frac{\partial}{\partial x_j}(\rho u_j) = 0 \\ \frac{\partial \rho u_i}{\partial t} + \frac{\partial}{\partial x_j}(\rho u_i u_j) = -\frac{\partial p}{\partial x_i} + \frac{\partial}{\partial x_j}(\tau_{ij}) \quad i = 1,2,3 \\ \frac{\partial \rho E}{\partial t} + \frac{\partial}{\partial x_j}((\rho E + p)u_j) = -\frac{\partial}{\partial x_j}(Q_j) + \frac{\partial}{\partial x_j}(\tau_{ij} u_i), \end{cases} \tag{4}$$

where ρ denotes the fluid density, u the velocity vector, p the pressure, ρE the total energy per unit mass, τ the total shear stress tensor (viscous and Reynolds shear stress) and Q the heat flux vector. The system of equations (4) is closed by the modified Spalart-Allmaras (SA-neg) model described in [1] to account for the effects of turbulent fluctuations in the mean flow. A second-order accurate Roe upwind scheme is employed for the spatial discretization, whereas a linearized Euler implicit scheme is used for time integration.

In the body-conformal region of the mesh, a wall-resolved approach is applied to capture the boundary layer, whereas the Musker wall law [11] is used to model the boundary layer of the immersed detail.

2.2.2 Application of the immersed boundary condition

In contrast to the classical body-fitted approach, imposing the boundary condition in the IBM region of the computational domain is not straightforward due to the staircase path of the mesh in the vicinity of the immersed obstacle. A special treatment is required to mimic the effects of the IB detail in flow. In our approach, the immersed boundary condition is imposed at target points using the flow state at the corresponding image points. Since image points are not discretization points of the mesh, the flow variables at image points are linearly interpolated using the gradient of the variables at the computed fluid cells including the image points. The gradient at these cells is reconstructed using the Green-Gauss method.

The pressure and the density are considered to be constant in the wall normal direction of a turbulent boundary layer, we then have $p_A = p_B$ and $\rho_A = \rho_B$ (where A is a target point and B is the corresponding image point). This LIBM approach is intended to be used for high-Reynolds number flows involved in aeronautical applications. To mitigate the additional cost of mesh resolution required to solve the viscous stress in a thin turbulent boundary layer, the Musker wall models[11] is used to reconstruct the no-slip boundary condition at IB wall points.

First, the friction velocity u_τ is evaluated at the IB image point and is used to reconstruct the tangential velocity u_t at the IB target point as follow:

$$u_{t,A} = u_\tau f\left(y_A^+\right), \text{ with } y_A^+ = \frac{y_A u_\tau}{\nu} \tag{5}$$

The normal velocity $u_{n,A}$ at target point A is computed by a linear interpolation as follow:

$$u_{n,A} = \frac{y_A}{y_B} u_{n,B} \tag{6}$$

Where y_A and y_B are the distances of points A and B to the immersed wall boundary.

Knowing the pressure, the density and the velocity at IB the target points, the total energy is computed at the IB target points by solving the third equation of (4) to account for compressibility effects. The pseudo-viscosity $\tilde{v}$ of the Spalart-Allamaras model is also evaluated at the IB target point A under the assumption of an equilibrium boundary layer, by solving following non-linear equation as described in [14]:

$$\tilde{\nu}^4 - \kappa u_\tau y \tilde{\nu}^3 - \kappa u_\tau y \nu^3 C_{v1}^3 = 0 \tag{7}$$

With y the distance between IB target points and the immersed obstacle and $\kappa = 0.41$ the Von Karman constant.

2.2.3 Extraction of skin quantities on the immersed walls

As the mesh does not conform the immersed obstacles shapes, it is not possible to directly extract the flow field quantities (pressure, density, turbulent viscosity, ...) at the computational domain nodes. These quantities are extracted at the IBM wall points at a given iteration similarly the flow field reconstruction at IBM target points as detail in section 2.2.2. The pressure and density at each IBM wall point is extrapolated from its corresponding image point, which leads to $p_W = p_B$ and $\rho_W = \rho_B$. The skin pressure and friction coefficients are then computed as follow :

$$C_p = \frac{p_W - p_\infty}{\frac{1}{2}\rho_\infty U_\infty^2} \tag{8}$$

$$C_f = \frac{\tau_\omega}{\frac{1}{2}\rho_\infty U_\infty^2} = \frac{\rho_W u_\tau^2}{\frac{1}{2}\rho_\infty U_\infty^2} \tag{9}$$

3 VALIDATION OF THE LOCAL IBM APPROACH

For the validation of the LIBM approach, we compute the turbulent flow past a 2D multi-element airfoil. The test case is taken from the NASA Turbulence Modeling Resource [13] and corresponds to a section of the full-scale NASA CRM-HL configuration with the chord-wise part located at $y = 16.256$ m. This configuration has been widely studied for verification and validation of CFD solvers using the body-fitted approach [7, 19]. The aim of this study is to demonstrate the ability of the LIBM approach to provide adequate simulation of the turbulent

flow past the multi-element airfoil with a significant reduction of the mesh generation effort. The simulation is performed with a Reynolds number of 5 million, a Mach number of 0.2 and an angle of attack of 16 degrees. The airfoil is sketched on Fig 2 where the solid line represents the main airfoil and the dashed lines represent the slat and the flap which will be immersed into the body-conformal mesh of the main airfoil.

Figure 2: Multi-element airfoil: main body (black solid line), immersed bodies (blue dashed lines)

3.1 Preprocessing steps

The first step of the preprocessing consists in performing a mesh adaptation of the initial body-conformal mesh of the main body airfoil, in order to properly capture the geometry and the flow physics induced by the immersed slat and flap (see Fig 3b). Then the blanking of the adapted mesh (see Fig 3c) and the location of IBM points is carried out following the procedure described in section 2.1.2. For this test case, the resolution close to IB is $h_c = 10^{-4}$ and the targeted y^+_{target} value at IB target points is 100.

3.2 Results

3.2.1 Grid convergence study and comparison with BF results

The first step in validating the LIBM approach is to compare LIBM results with a reference solution obtained on body-fitted mesh of the full multi-element profile. A grid convergence study is then performed to ensure that the discretization error decreases with increasing mesh resolution. For this purpose, CFD simulations are carried out on three different LIBM meshes with increasing mesh resolution and one body-fitted mesh. For LIBM meshes the first cell size in table 1 corresponds to the cell size close to the immersed obstacles. The mesh resolution over the main body where the BF approach is applied is $5 \cdot 10^{-6}$ for the three LIBM meshes.

Table 1: Meshes characteristics

Mesh	Body-fitted	LIBM coarse	LIBM medium	LIBM fine
Cell count	287 285	222 677	287 853	421 318
h_c	$5 \cdot 10^{-6}$	$5 \cdot 10^{-4}$	$1 \cdot 10^{-4}$	$5 \cdot 10^{-5}$

In Fig 4, a first qualitative good agreement is observed in the momentum flow field computed by the BF and LIBM approaches. Looking the streamlines trajectory, we can notice from the BF results that the turbulent boundary layer over the slat and the flap is mostly attached. This means that the Musker wall model, based on flat plate boundary layer assumptions should be able to properly reproduce the flow physics in the vicinity of the immersed slat and flap. A

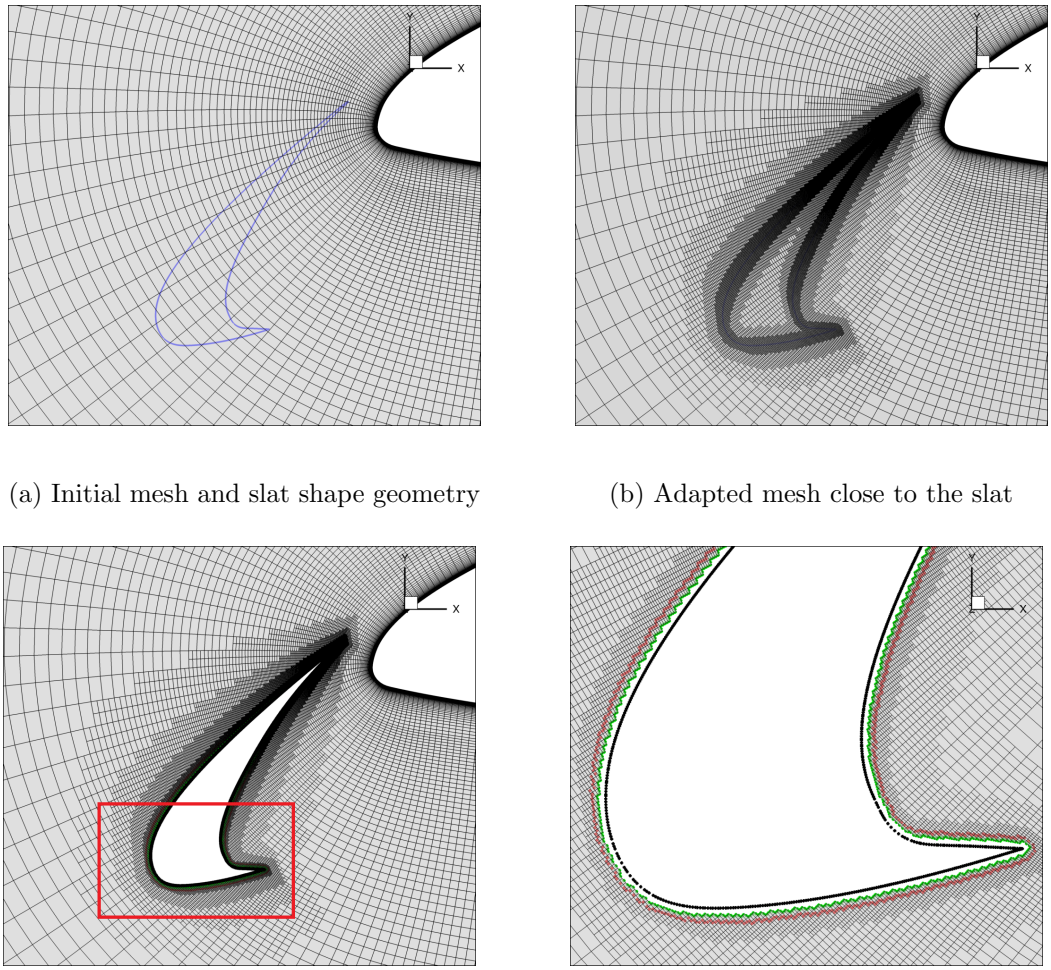

(a) Initial mesh and slat shape geometry

(b) Adapted mesh close to the slat

(c) Blanked mesh

(d) Zoom on the blanked mesh

Figure 3: IBM preprocessing steps for the slat

quantitative comparison of skin pressure and friction coefficient distributions shows an overall good agreement between the BF and LIBM approaches (Fig 5). A grid convergence is also observed as the C_p and C_f distributions obtained with the LIBM meshes become closer to the reference solution with increasing mesh resolution. Although the boundary layer is resolved with the same mesh resolution over the main body for both approaches, a zoom on the pressure coefficient shows a slight difference between the BF and LIBM solutions, especially at the leading edge. This is due to the difference in the slat wake captured by the BF and LIBM approaches, as the slat boundary layer is modelled in the LIBM approach and resolved in the BF approach. Fig 6 gives a clearer representation of pressure and skin friction coefficients distributions on the immersed details (slat and the flap). The wall model is well suited to reconstruct the velocities profiles when the boundary layer is attached and fully turbulent. However, at the leading edges (especially of the slat) the boundary layer is very thin and still laminar, therefore the wall model

is applied out of its validity domain. This explains why the two approaches differ the most at the leading edge of the slat (see Fig 6a and 6c).

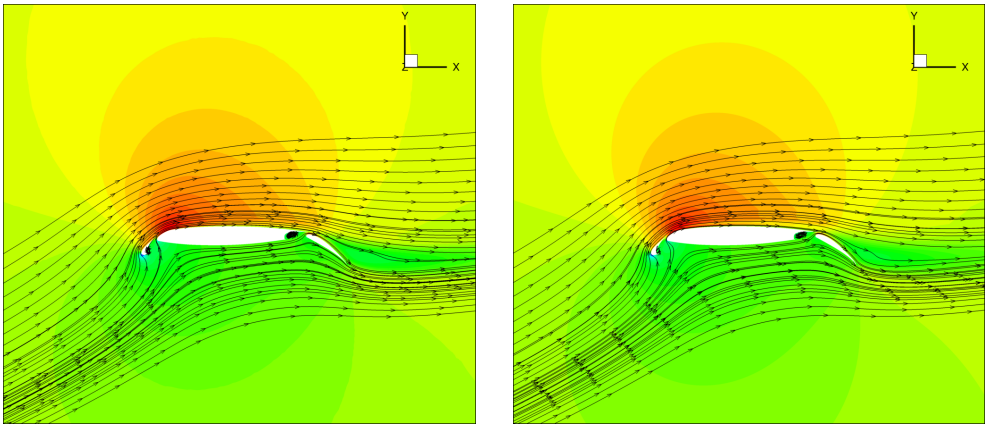

(a) Body-fitted approach (b) LIBM approach

Figure 4: Momentum field in the streamwise direction

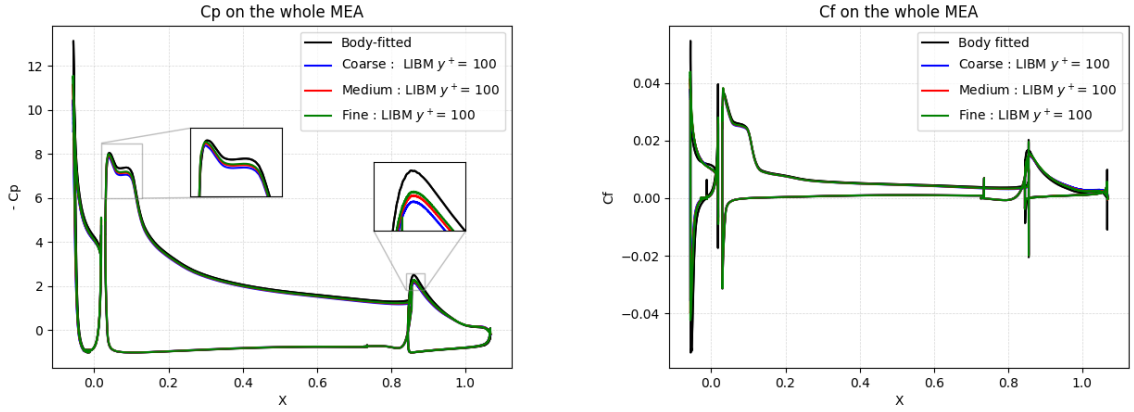

(a) Pressure coefficient (b) Skin friction coefficient

Figure 5: Skin pressure and skin friction coefficient over the whole profile

3.2.2 Comparison between local IBM and full IBM approaches

In this section, the efficiency of the LIBM approach compared to the traditional full IBM approach has been assessed. For the full IBM approach, CFD simulations are performed with the whole multi-element airfoil immersed in a Cartesian mesh. The mesh resolution for LIBM and full IBM approaches is the same in the vicinity of the immersed obstacle. Fig 7 shows an overall good agreement between the LIBM, the full IBM and the body-fitted approaches for

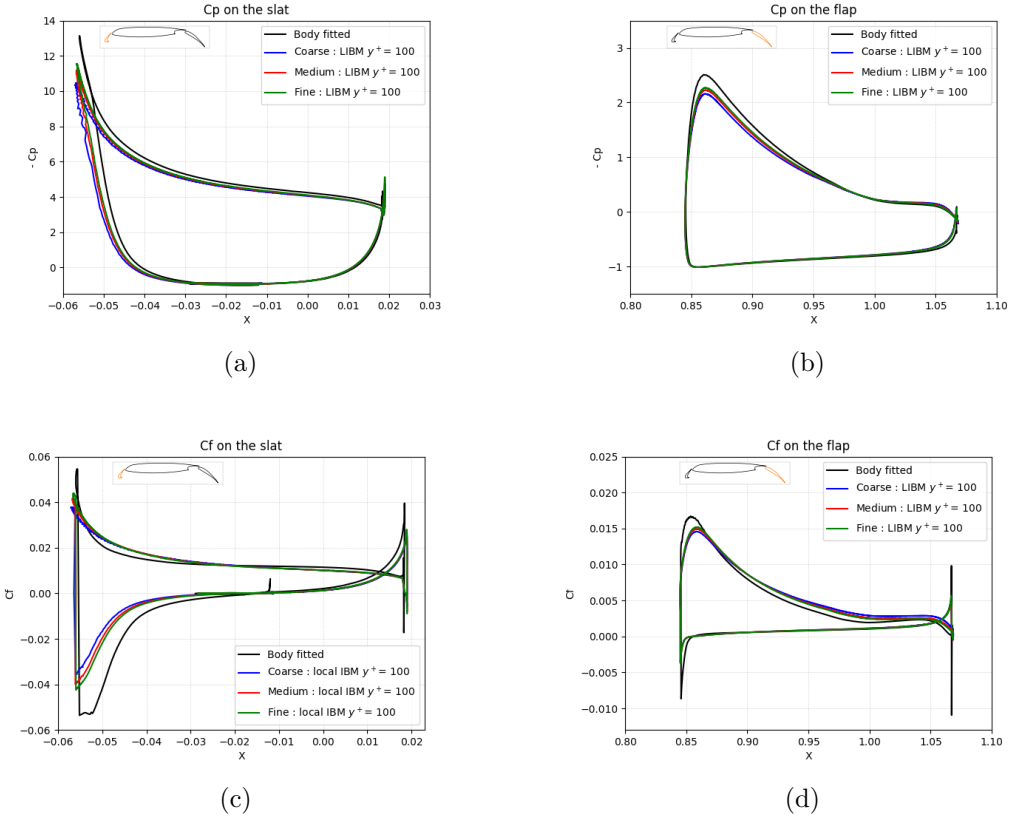

Figure 6: Skin pressure and friction coefficients on the slat and the flap

the skin pressure and friction coefficients over the entire multi-element airfoil. However, on the main body, the LIBM approach provides a slightly better result than the full IBM approach because the boundary layer is resolved with the LIBM approach and modelled with the full IBM approach. The application of a wall-resolved technique in the body-conformal region of the mesh also results in better prediction of integral coefficients (drag and lift) on the whole multi-element airfoil and therefore increases the solution accuracy of the LIBM approach compared to the full IBM approach. In tab 2, the error on the drag and lift coefficients is computed using the body-fitted result as the reference solution. This table shows that the coarse LIBM mesh predicts drag and lift coefficients more accurately than the medium full IBM mesh, even though the LIBM mesh has about 10 times less cells. This highlights the ability of the LIBM approach to take advantage of the strengths of the both body-fitted (good accuracy) and IBM (less mesh generation effort) approaches.

4 CONCLUSIONS

In this paper, a local application of the Immersed Boundary Method on body-conformal grids has been presented. This LIBM approach consists in using a classical body-fitted technique for simple geometry walls and to account for geometrical complex details thanks to IBM. An isotropic mesh adaptation is performed in the vicinity of the immersed obstacle to properly

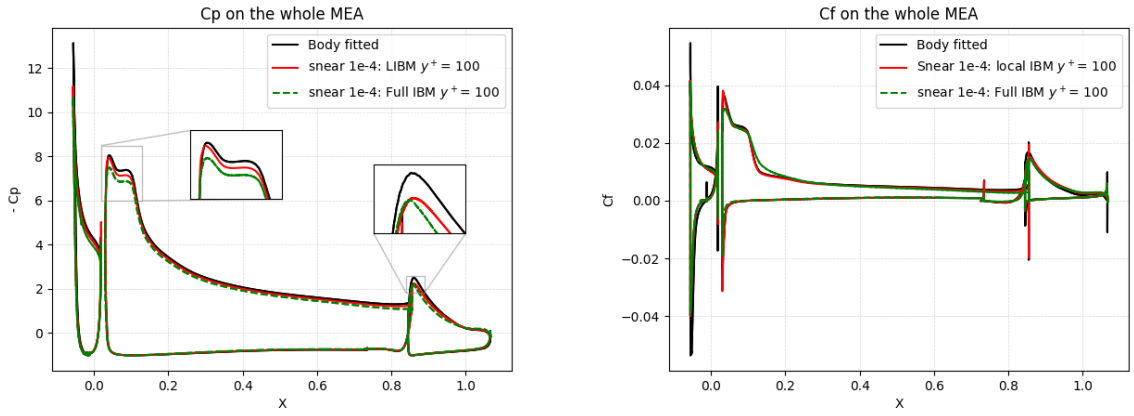

(a) Pressure coefficient

(b) Skin friction coefficient

Figure 7: Skin pressure and skin friction coefficient over the whole profile

Table 2: Integral coefficient on the whole airfoil

Mesh	Body-fitted	LIBM coarse	LIBM medium	LIBM fine	Full IBM medium
Cell count	287 285	222 677	287 853	421 318	2 173 016
Error on C_l (%)	0	4.24	3.12	2.49	6.9
Error on C_d (%)	0	11.55	8.6	7	14.08

capture the geometry and the flow physics near the immersed obstacle. This approach has been applied to simulate the turbulent flow past a 2D multi-element airfoil using compressible RANS simulation. Flow variables are forced at IB target points using turbulent boundary layer assumptions on a flat plate. Results obtained show that mesh convergence is achieved using the LIBM approach, which demonstrate the ability of this approach to reduce the discretisation error with increasing mesh resolution. A comparison between the LIBM solution and a reference solution computed on body-fitted mesh of the whole multi-element airfoil show a good agreement of the pressure and the skin friction distribution between the two approaches over the walls with an attached boundary layer. Furthermore, some comparisons between the local and global IBM approaches have highlighted the ability of the LIBM approach to provide a better prediction of the integral coefficients (lift and drag) with a significantly lower cell count compared to the global approach. The LIBM approach therefore seems to be an efficient tool to minimize the mesh generation effort while keeping a good solution accuracy. Further work will aim at validating this approach on 2D and 3D configurations involving a detached boundary layer.

References

[1] Steven R Allmaras and Forrester T Johnson. “Modifications and clarifications for the implementation of the Spalart-Allmaras turbulence model”. In: *Seventh international conference on computational fluid dynamics (ICCFD7)*. Vol. 1902. Big Island, HI. 2012.

[2] C. Benoit, S. Péron, and S. Landier. "Cassiopee: a CFD pre-and post-processing tool". In: *Aerospace Science and Technology* 45 (2015), pp. 272–283.
[3] Francesco Capizzano. "Turbulent wall model for immersed boundary methods". In: *AIAA journal* 49.11 (2011), pp. 2367–2381.
[4] B. Constant et al. "An improved immersed boundary method for turbulent flow simulations on Cartesian grids". In: *Journal of Computational Physics* 435 (2021), p. 110240.
[5] Ever A Fadlun et al. "Combined immersed-boundary finite-difference methods for three-dimensional complex flow simulations". In: *Journal of computational physics* 161.1 (2000), pp. 35–60.
[6] Liang Ge and Fotis Sotiropoulos. "A numerical method for solving the 3D unsteady incompressible Navier–Stokes equations in curvilinear domains with complex immersed boundaries". In: *Journal of computational physics* 225.2 (2007), pp. 1782–1809.
[7] Todd Michal et al. "Comparing unstructured adaptive mesh solutions for the high lift common research airfoil". In: *AIAA journal* 59.9 (2021), pp. 3566–3584.
[8] Rajat Mittal and Gianluca Iaccarino. "Immersed boundary methods". In: *Annu. Rev. Fluid Mech.* 37 (2005), pp. 239–261.
[9] Loıc Mochel, Pierre-Élie Weiss, and Sébastien Deck. "Zonal immersed boundary conditions: application to a high-Reynolds-number afterbody flow". In: *AIAA journal* 52.12 (2014), pp. 2782–2794.
[10] Parviz Moin. "Advances in large eddy simulation methodology for complex flows". In: *International journal of heat and fluid flow* 23.5 (2002), pp. 710–720.
[11] Antony J Musker. "Explicit expression for the smooth wall velocity distribution in a turbulent boundary layer". In: *AIAA Journal* 17.6 (1979), pp. 655–657.
[12] Kazuhiro Nakahashi. "Immersed boundary method for compressible Euler equations in the building-cube method". In: *20th aiaa computational fluid dynamics conference*. 2011, p. 3386.
[13] *NASA Turbulence Modeling Resource*. URL: `https://turbmodels.larc.nasa.gov/`.
[14] S. Péron et al. "An immersed boundary method on Cartesian adaptive grids for the simulation of compressible flows around arbitrary geometries". In: *Engineering with Computers* 37.3 (2021), pp. 2419–2437.
[15] Charles S Peskin. "Flow patterns around heart valves: a numerical method". In: *Journal of computational physics* 10.2 (1972), pp. 252–271.
[16] F Roman et al. "An improved immersed boundary method for curvilinear grids". In: *Computers & fluids* 38.8 (2009), pp. 1510–1527.
[17] Yoshiharu Tamaki, Motoshi Harada, and Taro Imamura. "Near-wall modification of Spalart–Allmaras turbulence model for immersed boundary method". In: *AIAA journal* 55.9 (2017), pp. 3027–3039.
[18] Yu-Heng Tseng and Joel H Ferziger. "A ghost-cell immersed boundary method for flow in complex geometry". In: *Journal of computational physics* 192.2 (2003), pp. 593–623.
[19] Carmen-Ioana Ursachi et al. "Output-based adaptive RANS solutions using higher-order FEM on a multi-element airfoil". In: *Aiaa Aviation 2020 Forum*. 2020, p. 3220.
[20] P. Volpiani et al. "Simulating the Common Research Model using the new CFD software from ONERA, DLR and Airbus". In: *AIAA AVIATION 2023 Forum*. 2023, p. 3275.
[21] Wei Jun Zhu et al. "Hybrid immersed boundary method for airfoils with a trailing-edge flap". In: *AIAA journal* 51.1 (2013), pp. 30–41.